JOURNAL OF CATALYSIS **166,** 324–332 (1997)
ARTICLE NO. CA971510

Reaction Kinetics of Methane Oxidation over $LaCr_{1-x}Ni_xO_3$ Perovskite Catalysts

M. Stojanović,* C. A. Mims,*[,1,2] H. Moudallal,† Y. L. Yang,† and A. J. Jacobson†

*Department of Chemical Engineering and Applied Chemistry University of Toronto, Toronto, Ontario M5S 3E5, Canada; and †Department of Chemistry, University of Houston, Houston, Texas 77204-5641

Received July 8, 1996; revised September 24, 1996; accepted October 30, 1996

Ternary perovskite oxides $LaCr_{1-x}Ni_xO_3$, ($x = 0$ to 1.0) were evaluated as methane oxidation catalysts over the temperature range 300–500°C and as a function of the partial pressures of oxygen and methane (12–90 kPa). All catalysts are stable in oxygen containing atmospheres, while oxygen starvation causes destructive reduction to Ni metal for $x > 0.5$. The catalytic activity increases monotonically with the value of x. The nonseparable (composition, temperature) kinetics behavior is well correlated by an oxidation–reduction mechanism for all catalysts. Based on the observed nonlinear increase in catalytic activity with nickel content, Ni–O–Ni ensembles are proposed as the key surface reagent.

INTRODUCTION

Simple perovskites with the basic formula ABO_3 have been extensively investigated as catalysts (1–4) since it was recognized that oxides could compete with metals in oxidation reactions (5–8). The majority of studies have focused on oxidation catalysis, although their use in other reactions has also been reported. The perovskite lattice tolerates wide variations in the identities of the A and B cations and provides a robust host for a large number of substitutions involving either or both cation sites. This flexibility testifies to the unusual stability of the structure and allows deliberate variation in surface and bulk properties for individual applications. These same compounds provide unmatched opportunities to examine structure/property relationships in a controlled manner.

The early lanthanide perovskites (particularly $A = La$, $B =$ first-row transition metal) have received the most attention for oxidation catalysis, particularly in catalytic combustion for environmental applications (destruction of hydrocarbons, CO, NO). The thermodynamic stability to reduction of the series of binary oxides $LaBO_3$ decreases along the sequence $B =$ Cr to Ni (9, 10). A general correlation between the catalytic activity of the various materials and the ease of reduction, both thermodynamic and kinetic, has been found in many of these studies, conforming to a persistent theme in oxide catalysis (11). For example, studies of methane oxidation over the binary oxides $LaBO_3$ (12–15) show catalytic activity increasing across the series ($B =$ Cr to Co) with $LaCrO_3$ the least active. The reported activity of $LaNiO_3$ relative to this series differs among the various studies, from apparently being the most active (15), to somewhat less active than $LaCoO_3$ (12) to almost as poor as $LaCrO_3$ (13). This situation for CO oxidation activity (12, 16–19) is similar, with $LaCoO_3$ the most active and $LaNiO_3$ either similar (17) or inferior (12) in activity. The presence of extraneous phases is a persistent problem in obtaining quantitative catalytic data (15, 20–23) and probably explains some of the variability in results. Modification of the surface activity of these materials during the reaction has also been noted (15). The identity of the A cation is clearly a significant factor in determining the catalytic activity (19, 22, 24); for example, $NdCoO_3$ is superior to $LaCoO_3$ (22) in methane oxidation. Generally, however, the identity of the B cation has a larger influence.

$LaBO_3$ oxidation catalysts can be improved by substitutions on A and/or B sites. Partially substitution of La by Sr, Ca, or Ba increases oxide ion mobility, reducibility, and catalytic rates (12, 13, 15, 20, 23, 25–28). Optimum A site compositions levels are typically $La_{0.8}Sr_{0.2}$ for both CO and hydrocarbon oxidations. Substitutions of Sr for La in La_2NiO_4 also increases methane oxidation rates (29). Substitutions on the B site have also received some attention. Inclusion of 10% Ni or Co on the B sites in $La_{0.8}Sr_{0.2}CrO_3$ produces increased oxygen availability and methane oxidation rates (30). Cu substitution in $LaMO_3$ ($M =$ Fe, Mn, Co) increased CO oxidation rates (23). Other doubly substituted (A and B) perovskites have been tested (21, 27, 31–35) and synergistic effects (superior performance of the mixed B, B' materials over the end members) reported in some cases (31). In many of these studies, catalytic rates were examined at a single gas composition or only in terms of light-off temperatures—full kinetic studies of reaction orders were obtained only in a minority of cases.

[1] To whom correspondence should be addressed.
[2] Fax: (416) 978-8605. E-mail: Mims@ecf.toronto.edu.

0021-9517/97 $25.00

No systematic study of the catalytic reaction kinetics of a complete $La(B, B')O_3$ series has been reported.

In addition to surface catalytic properties, other materials properties (electronic and ionic conductivity, magnetic properties, and thermodynamic properties) are affected by compositional changes. The simultaneous optimization of several properties is necessary for membrane catalysts based on mixed ionic/electronic conductivity (36, 37) and for solid oxide fuel cell components (38–42). Not only are substituted perovskites used in the current SOFC technology as cathode and interconnect material (38, 43), but new electrolytes (44, 45) and anode materials (40, 41) with the perovskite structure are being investigated. Our interest is in the latter application. Nickel substitutions in $LaCrO_3$ allows the use of this reductively robust lattice as a host, while increasing the catalytic activity and conductivity (46, 47). In this paper steady-state methane oxidation kinetics are reported for the substitional series $LaCr_{1-x}Ni_xO_3$. The synthesis, structure, stability, and surface composition of this series of oxides are described in an accompanying paper (48).

EXPERIMENTAL METHODS AND MATERIALS

Catalytic Materials

A brief summary of the materials and their pertinent characteristics is included in Table 1. Duplicate syntheses (denoted *A* and *B*) of the series $LaCr_{1-x}Ni_xO_3$ ($x = 0$, 0.25, 0.50, 0.75, 1.0) produced single-phase (by XRD) perovskite powders for the catalytic studies. Additional reference materials (denoted *C*) were also produced, largely to examine the role of small quantities of other phases (invisible by XRD) which can arise with small deviations from perfect stoichiometry or incomplete mixing in the synthesis of mixed oxides. The reference catalysts included the unary oxides (La_2O_3, Cr_2O_3, NiO), a perovskite with intentionally added NiO (*C*2) and one which was destructively reduced to produce multiphase materials (*C*3), La_2NiO_4, and a sample produced with excess lanthanum (50%) in the original Pechini solution (*C*1). This latter method assures complete incorporation of the "*B*" cations into mixed metal oxides during gelation and calcination. Subsequent leaching in citric acid removed nonperovskite materials.

TABLE 1

Materials Used in This Study

#	Nominal composition	Surface Ni (Ni + Cr)	Surface area $m^2\ g^{-1}$
A0	$LaCrO_3$	0	3.3
A25	$LaCr_{0.75}Ni_{0.25}O_3$	0.28	2.5
A50	$LaCr_{0.5}Ni_{0.5}O_3$	0.44	3.5
A75	$LaCr_{0.25}Ni_{0.75}O_3$	0.70	2.9
A100	$LaNiO_3$	1	3.3
B0	$LaCrO_3$	0	4.9
B25	$LaCr_{0.75}Ni_{0.25}O_3$	0.19	6.6
B50	$LaCr_{0.5}Ni_{0.5}O_3$	0.47	8.6
B75	$LaCr_{0.25}Ni_{0.75}O_3$	0.71	7.9
B100	$LaNiO_3$	1	8.1
C1	$LaCr_{0.5}Ni_{0.5}O_3$	0.32	6.1
C2	NiO + B75	0.76	4.2
LA	La_2O_3	—	3.0
CR	Cr_2O_3	—	5.9
NI	NiO	—	1.3

Note. Details are in Ref. (48).

Methane Oxidation Kinetics

Steady-state catalytic methane oxidation rates were measured using a downflow tubular quartz reactor (quartz, 4 mm i.d.) operated near one atmosphere total pressure with gas chromatographic (MTI M200) analysis. The GC, the flow meters (MKS 1159B) for the feed components, and the furnace were all under computer control. For the catalysis studies, the calcined powders were pressed into pellets, crushed, and sieved to desired particle sizes (75–150 μm diameter). Fresh catalyst charges of 0.20–0.30 g were supported on an integral quartz frit and a thermocouple in a quartz sheath was maintained in contact with the catalyst charge. The resulting flow restriction together with a similar one downstream accompanied by addition of inert gas serves to minimize the gas residence time at reaction temperature. Initially, the catalytic activities of all materials were screened during one or more heating and cooling cycles at one gas composition ($CH_4 : O_2 : He = 2 : 1 : 5$) with rate measurements at defined temperature intervals (25 or 50°C). Subsequently, the gas composition dependence was measured for all materials over the temperature range 300–550°C by varying the methane (oxygen) partial pressure (12.5–87.5 kPa) at a fixed oxygen (methane) partial pressure of 12.5 kPa. A constant total flow rate (40 mL/min at ambient) was maintained during these experiments. The importance of product species in the rate law was tested by gas residence time variation at one gas composition and various temperatures. Thiele modulus calculations and experimental data over a range of particle sizes show that mass transport limitations did not influence the reaction kinetics at temperatures less than 500°C and particle sizes 75–150 μm in diameter.

RESULTS AND DISCUSSION

Catalytic Kinetics: General Observations

Figure 1 shows the results of the temperature-programmed reaction in a methane–oxygen mixture ($CH_4 : O_2 : He = 1 : 1 : 6$) for several $La(Cr, Ni)O_3$ catalysts. Two distinct regions are apparent: the first, catalytic combustion to CO_2 and H_2O, becomes significant between 350 and 600°C and is the main focus of this paper. A general increase in the conversion with nickel content at a given

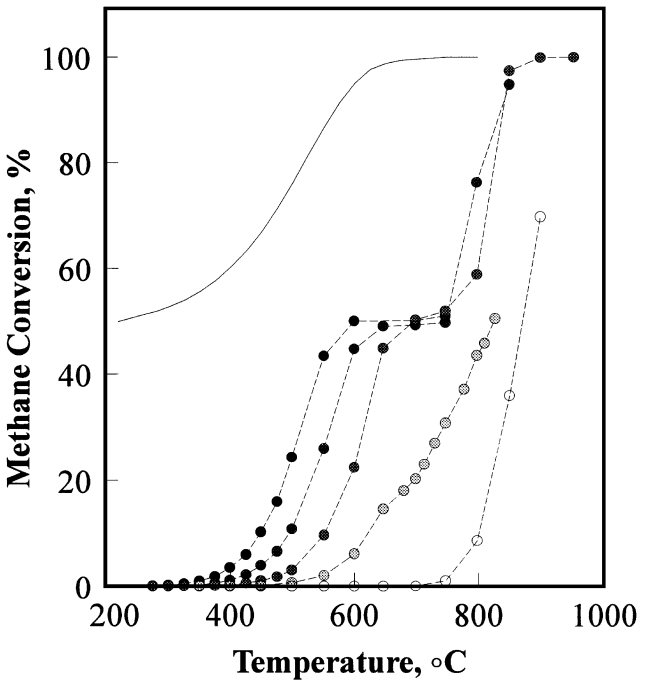

FIG. 1. Methane conversion as a function of temperature, 100 kPa total pressure $CH_4 : O_2 : He = 1 : 1 : 6$, total flow 80 mL/min ambient: O = empty reactor, shaded circles = $LaCr_{1-x}Ni_xO_3$ catalysts $x = 0.0$, 0.25, 0.75, and 1.00 (all 0.20 g), in increasing order of conversion and depth of shading. The thermodynamic limit is given by the solid line.

temperature is apparent in Fig. 1. Methane conversion by complete combustion is limited to 50% by oxygen starvation at this gas composition, however, further methane conversion by the reforming reactions with the H_2O and CO_2 combustion products is thermodynamically possible at higher temperatures (above 650°C) and becomes significant in the second, high-temperature (above 750°C) region. At the cooler end of the reforming region (650 to 750°C), low selectivities (<.05%) to ethane and ethylene were observed, indicating that small quantities of gas phase methyl radicals are formed by surface reactions under these conditions. The C_2 selectivities drop to undetectable amounts (<10 ppm) at higher temperatures. Carbon deposition is thermodynamically possible over various ranges of composition and temperature sampled in this study, and was observed in our experiments at the highest temperatures (>850°C) only in methane-rich gas mixtures ($CH_4/O_2 > 2$). In parallel with increased methane reactivity, carbon deposition was also observed to be more facile on the nickel-rich materials, and plugged the reactor on two occasions over materials with high nickel content. No carbon deposition was observed on $LaCrO_3$ under any of the reaction conditions.

Catalyst Stability

The ternary perovskites were all stable methane oxidation catalysts except under two circumstances: (a) mild deactivation was observed for most catalysts during the first exposure to methane combustion conditions and (b) major changes to the nickel-rich materials occurred due to destructive reduction under oxygen starvation. Typically, mild deactivation by up to 50% was observed in the rates measured at 400°C after the first temperature cycle of catalyst screening even when the maximum reaction temperatures (650°C) were kept well below the 760°C calcination temperatures and oxygen starvation was avoided. A somewhat larger average decrease in rates occurred for the nickel-poor samples than for the nickel-rich ones. This initial deactivation was accompanied by small decreases in surface area, which accounted for some, but not all of the rate decrease, indicating some rearrangement of the surface during the initial exposure. Similar changes were noted in previous studies of binary perovskites (15). No changes in XRD or XPS were observed as a result of the rate decrease. Nor were changes detected in the surface compositions after exposure to high temperatures (500°C) in vacuum or after extensive use as a methane oxidation catalyst at temperatures up to 600°C, again provided that the reaction did not proceed to oxygen starvation. Subsequent cycles gave stable reproducible rates and surface areas over several days. Furthermore, reductions in the surface areas of these materials by higher-temperature calcination resulted in proportional decreases in rate, indicating stable rates-per-unit surface area. These stable "run-in" rates were used for kinetic analysis below. Under oxygen starved conditions at high temperatures, $LaNiO_3$ decomposed, the catalyst plugged with carbon at 850°C, and La_2NiO_4 and NiO were visible by XRD in the recovered material which had been cooled in methane–oxygen mixtures.

Methane Combustion Kinetics

Table 2 summarizes the catalytic results for all the materials tested. Data obtained under differential conditions with conversions of the limiting reagent less than 10% were included in the kinetic analysis.

Catalyst screening: dependence on catalyst composition. The rates of methane combustion at one standard reaction condition (400°C, $CH_4 : O_2 : He = 2 : 1 : 5$) are shown in Fig. 2. A general, scattered increase is seen with increasing nickel content. The error bars in Fig. 2 indicate the repeatability of the rates for the same catalyst preparation and include all measured rates after the first temperature cycle. Different symbols distinguish the *A* and *B* preparative series. Also included are the rates measured for the reference catalysts. These rates are consistent with previously published data for the end members and reference catalysts. Previously published data for $LaCrO_3$ and $LaNiO_3$ (13, 15) are shown in Fig. 2. These values, obtained at lower methane partial pressures than ours, were extrapolated to our conditions using our rate laws discussed below, and the agreement is satisfactory. Interestingly, the

TABLE 2

Kinetic Parameters for Methane Oxidation

Catalyst		2:1:5 Rate parameters[a]		Model rate parameters[b]				
#	Nominal composition	log (A/μmol s^{-1} m^{-2})	E/kJ/mol	log (A_c/μmol s^{-1} m^{-2} atm^{-1})	E_c kJ/mol	log (A_o/μmol s^{-1} m^{-2} atm^{-1})	E_o/kJ/mol	Fit[c] %
A0	$LaCrO_3$	5.37	101	6.14	97	—	—	12
A25	$LaCr_{0.75}Ni_{0.25}O_3$	5.48	90	6.25	94	9.96	131	7
A50	$LaCr_{0.5}Ni_{0.5}O_3$	5.67	109	7.86	102	8.33	105	12
A75	$LaCr_{0.25}Ni_{0.75}O_3$	6.29	93	7.16	99	7.67	95	16
A100	$LaNiO_3$	6.46	95	7.80	98	8.25	99	8
B0	$LaCrO_3$	7.05	108	6.15	89	10.19	128	19
B25	$LaCr_{0.75}Ni_{0.25}O_3$	6.13	100	6.04	89	8.22	109	10
B50	$LaCr_{0.5}Ni_{0.5}O_3$	6.52	100	6.90	94	8.13	104	6
B75	$LaCr_{0.25}Ni_{0.75}O_3$	6.15	96	6.75	92	7.62	99	5
B100	$LaNiO_3$	6.00	86	7.01	88	7.41	88	5
C1	$LaCr_{0.5}Ni_{0.5}O_3$	5.99	98	6.55	94	8.38	111	8
C2	$NiO + B75$	7.42	98	6.84	93	8.48	109	9
LA	La_2O_3	8.70	139	—	—	—	—	—
CR	Cr_2O_3	7.15	108	—	—	—	—	—
NI	NiO	7.44	99	9.33	107	8.23	95	14

[a] Rate at $CH_4:O_2:He = 2:1:5$ (100 kPa) $= A \exp\{-E/RT\}$.
[b] $k_c = A_c \exp\{-E_c/RT\}$, similarly for k_o (see text).
[c] Standard deviation of model fit.

nickel-poor samples (including $LaCrO_3$) which showed somewhat greater initial deactivation also showed more rate variability between sample preparations. NiO has a similar, somewhat higher specific activity compared to $LaNiO_3$, in agreement with previous measurements (14, 15) while the specific rates for Cr_2O_3 and La_2O_3 bracket our observed values for $LaCrO_3$. La_2NiO_4 has a low specific activity similar to that for La_2O_3, in agreement with previous data (14, 15). The Arrhenius parameters for each catalyst in this gas mixture are listed in Table 2. The activation energies are in general agreement with previously published values: 120 (13) and 142 (15) kJ/mol for $LaCrO_3$, 81 (13) and 79 (15) kJ/mol for $LaNiO_3$, 100 kJ/mol for NiO, and 101 kJ/mol for Cr_2O_3 (15). The activation energies depend somewhat on gas composition, as discussed below. The rates of the multiphase reference catalysts (see Table 2) show that adding NiO to $LaCr_{0.25}Ni_{0.75}O_3$ (sample C2) results in a small decrease in the rate despite the addition of nickel. Similarly, the destructively reduced material showed little change in reactivity. Finally, the $LaCr_{0.50}Ni_{0.50}O_3$ (C1) material prepared with excess La showed a rate consistent with its surface nickel content and this rate is also included in Fig. 2.

Kinetic analysis. Different rate laws for methane oxidation hold for each catalyst composition over the range of conditions. Furthermore, the rate laws are not separable, i.e., for most of the catalysts, there is coupling between the gas composition dependence and the temperature dependence (the apparent activation energy depends on gas composition and the effective reaction orders depend on temperature). Thus, although the trend apparent in Fig. 2 holds over the relevant range of gas compositions and temperatures, the quantitative dependence of rate on catalyst composition depends on the reaction conditions. An analysis of these aspects is necessary prior to a quantitative description of the effect of nickel content. A power law rate expression,

$$r = k P_{CH_4}{}^n P_{O_2}^m, \qquad [1]$$

provides adequate fits ($r^2 \geq 0.98$) to the data over the range of conditions here and is used to correlate the data. For all materials, the effective methane reaction orders, n, are larger (0.5 to 1) than the oxygen orders, m, (0 to 0.25). The following trends were observed:

(1) the methane and oxygen orders are generally anticorrelated: higher methane orders are associated with lower oxygen orders and vice versa. Figure 3 illustrates this trend with the raw data for $LaCr_{0.75}Ni_{0.25}O_3$, the lines are fits by the redox model discussed below;

(2) the methane orders are lower and oxygen orders generally higher for the materials with higher nickel content at the same temperature; and

(3) the oxygen pressure dependences generally become weaker, while the corresponding methane dependences become stronger with increasing temperature.

As a corollary to point (3), the activation energies which fit the data are generally lower in oxygen rich reactant mixtures (associated with lower oxygen reaction orders) than in methane rich compositions. Points (2) and (3) are illustrated

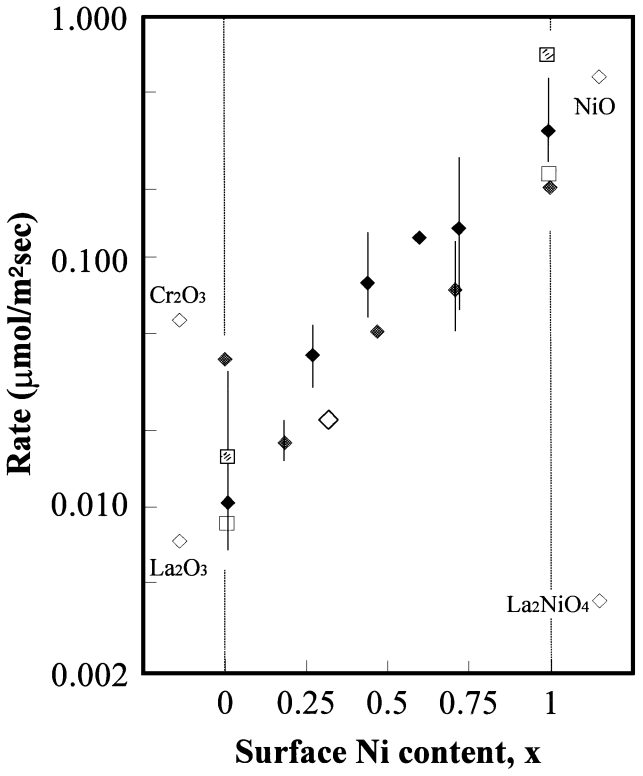

FIG. 2. Reaction rates as a function of surface composition $x = \mathrm{Ni}/(\mathrm{Cr} + \mathrm{Ni})$ at a single reaction condition (400°C, 100 kPa total pressure $CH_4 : O_2 : He = 2 : 1 : 5$, 0.20 g catalyst, total flow 80 mL/min): diamonds are the $LaCr_{1-x}Ni_xO_3$ materials (solid = A series, shaded = B series, open = C series). Reference compounds are shown by open diamonds outside $0 < x < 1$ field and are labeled. Results from previous studies are squares (open, Ref. (13); shaded, Ref. (15)) and were extrapolated to our conditions using our rate laws (see text).

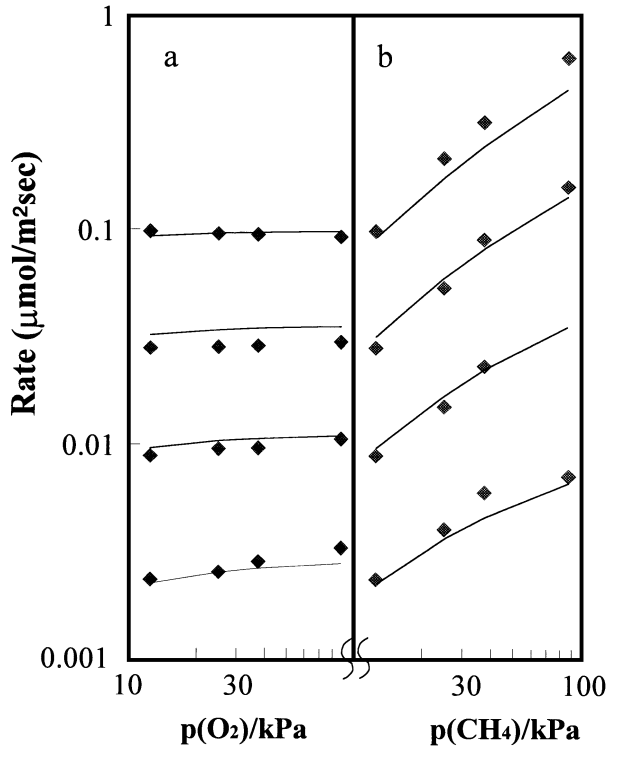

FIG. 3. Reaction rates as a function of gas composition for $LaCr_{0.75}Ni_{0.25}O_3$: panel (a) $P(CH_4) = 12.5$ kPa, panel (b) $P(O_2) = 12.5$ kPa; data in each are for $T = 350$°C, 400°C, 450°C, 500°C in increasing order of rate; lines are model fit (parameters in Table 2) described in the text.

in Fig. 4 for the catalysts ($x = 0.0$, 0.25, 0.50, and 0.75, 1.00) and temperatures between 300 and 500°C. The behavior of $LaNiO_3$ does not quantitatively continue the trend, and the effective reaction orders show a weaker temperature dependence. The dashed line in Fig. 4 indicates the trend seen for $LaNiO_3$—the data points have been omitted for clarity. Figure 5 plots the effective orders in methane against those for oxygen. The anticorrelation of methane and oxygen dependences for the $LaCr_{1-x}Ni_xO_3$ materials is scattered, but apparent. Results for two of the reference compounds (NiO and C2) are also included. The solid line is predicted by the analysis below. The distinct behavior of NiO, compared to the perovskites and the Ni-impregnated material, indicates a negligible contribution by extraneous NiO in the perovskite-catalyzed rates. Even the perovskite with intentionally added NiO exhibits similar kinetics to the perovkites despite NiO being evident in XRD. A redox mechanism such as that originally proposed by Mars and van Krevelen (MVK) (49) provides a rational explanation of the observed behavior. According to MVK, the catalysis is accomplished by alternating, irreversible reduction and

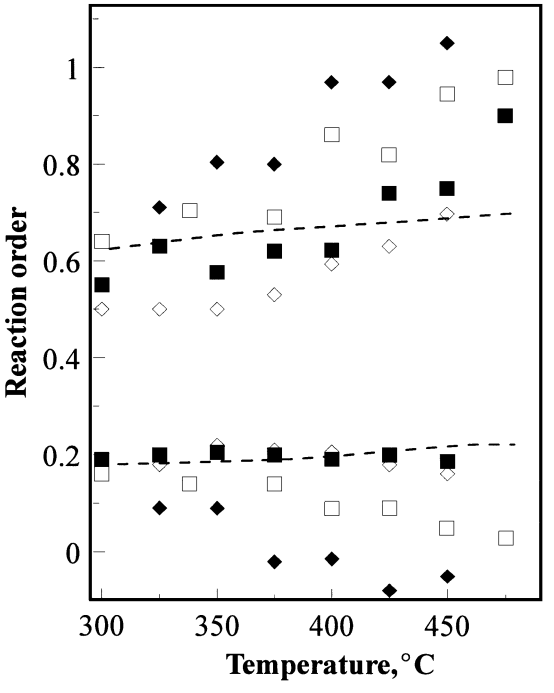

FIG. 4. Reaction orders (methane, upper group; oxygen, lower group) as a function of temperature for the catalyst series $LaCr_{1-x}Ni_xO_3$ ($x = 0.0$ (◆), 0.25 (□), 0.50 (■), 0.75 (◇), 1.00 (- - - -)).

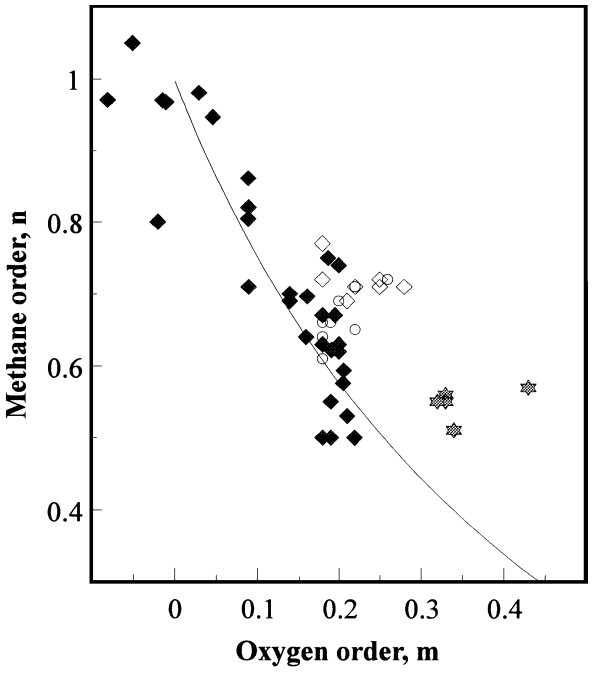

FIG. 5. Methane reaction orders plotted against oxygen orders: ◆ = data from Fig. 4 ($x = 0.0$ to 0.75), ○ = $LaNiO_3$, ◇ = NiO + $LaCr_{0.25}Ni_{0.75}O_3$(C2), ✡ = NiO. Solid line is predicted by model described in the text ($\alpha = 1$, $\beta = 1$).

oxidation reactions at surface sites represented by the two unbalanced (multistep, nonelementary) reactions below,

$$CH_4 + \underline{O} \rightarrow \text{Products} + \_\_, \qquad \text{rate} = r_c = r_c^o\theta \qquad [2]$$

$$O_2 + \_\_ \rightarrow \underline{O}, \qquad \text{rate} = r_o = r_o^o(1-\theta), \qquad [3]$$

where $\_\_$ and $\underline{O}$ represent reduced and oxidized sites, respectively, and θ is the fraction of the sites which are oxidized. The observed rate is related to the maximum intrinsic rates, r_c^o (all sites oxidized) and r_o^o (all sites reduced) of the two processes, by

$$1/r_{obs} = 1/r_c^o + 1/r_o^o. \qquad [4]$$

If one process is inherently much slower than the other, the rate law for the slow step will determine the observed rate law for the overall process. If neither can be neglected then the observed rate law is determined by both sets of kinetic parameters in accordance with Eq. [4]. It is easy to show that if the two processes have the following rate laws

$$r_c^o = k_c P_{CH_4}^{\alpha} \qquad [5]$$

and

$$r_o^o = k_o P_{O_2}^{\beta} \qquad [6]$$

that the observed effective orders, n and m, taken around a single composition are given by the expressions

$$n = \alpha\left[1 - r_c^o/\left(r_c^o + r_o^o\right)\right] \qquad [7]$$

and

$$m = \beta\left[1 - r_o^o/\left(r_c^o + r_o^o\right)\right]. \qquad [8]$$

When taken over a finite range of partial pressures, of course, this model predicts curved order plots as shown in Fig. 3. Single orders which best fit the data over the partial pressure range are predicted to follow the solid line in Fig. 5 if the rate laws in Eqs. [5] and [6] are first order ($\alpha = \beta = 1$). Good fits to all the data were obtained with this simple model, with simple Arrhenius expressions for k_c and k_o. The procedure for each catalyst (and for each α, β combination) involved first obtaining the best values of k_c and k_o, according to Eqs. [4]–[6] at each temperature followed by fitting these values over the temperature range to obtain Arrhenius parameters. Since the methane orders were near unity when the oxygen orders were near zero, α was always assumed to be unity and values of $\beta = 1$ and 0.5 were examined. If the values of α and β were constrained to be the same for all the catalysts, the best fits were obtained with $\alpha = \beta = 1$ and these optimum rate constant parameters are included in Table 2. The rates predicted with these parameters reproduce every experimental data point to within 20% (worst point) with no systematic deviations. The standard deviations between model and experiment are listed for each catalyst in Table 2. Close scrutiny of the data reveals that the model fails in minor ways to reproduce the data. For example, the oxygen orders for $x = 0.5$ and 0.75 in Fig. 3 do not decrease as rapidly with temperature as expected from the increase in methane orders. Such discrepancies produce the scatter visible in Fig. 5. Nevertheless, a large part of the coupling between the gas composition and temperature dependences is explained by this model.

A consistent picture emerges from this interpretation of the data. For the chromium-rich catalysts, methane orders near unity and oxygen orders near zero imply that methane activation is the limiting process. The rates of both processes increase with increasing nickel content at a given temperature, but the methane activation increases more rapidly, so that site reoxidation becomes increasingly limiting for the nickel-rich catalysts resulting in lower methane orders and non-zero oxygen orders. Furthermore, a higher activation energy for site oxidation (k_o) than for methane activation (k_c) results in the trend toward $n = 1$, $m = 0$ at higher temperatures as well as the lower activation energies in oxygen-rich reactants, especially apparent in the nickel-poor materials.

Correlation of Kinetics with Catalyst Composition

With this analysis it is possible to discuss quantitatively the trends in the reactivity of these materials with

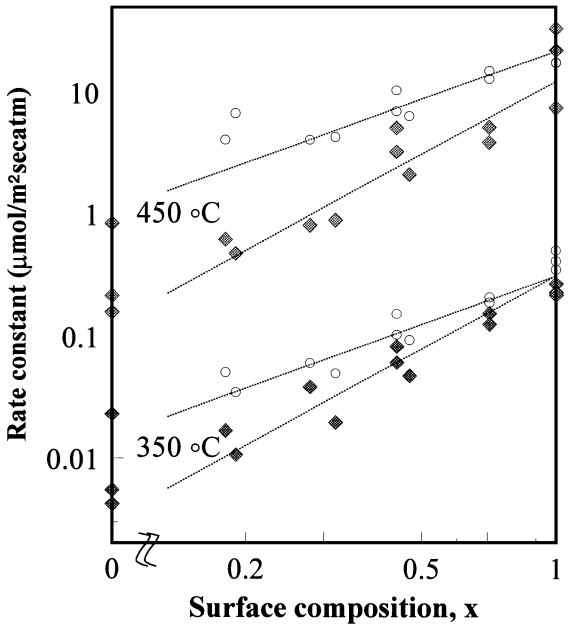

FIG. 6. Model rate constant parameters k_c (diamonds) and k_o (circles) derived from the data as a function of composition parameter, x in $LaCr_{1-x}Ni_xO_3$: upper grouping at 450°C, lower grouping at 350°C. Lines through k_c are quadratic ($k \propto x^2$) and through k_o are linear ($k \propto x$).

composition. Figure 6 shows how the rate constants derived from the model depend on composition for two temperatures. The methane activation rate constants, k_c (filled symbols), increase on average even more rapidly than the overall rate with increasing amounts of nickel, since site reoxidation becomes more limiting for the nickel-rich materials. The lines drawn through the data represent a quadratic response to the surface nickel concentration. This provides a reasonable fit, although contributions by the chromium content of the surface obviously cannot be ignored (the values for $LaCrO_3$ are shown on the left-hand edge of Fig. 6). The site oxidation rate coefficients, k_o (open symbols), show a weaker but still positive response to increasing nickel content. Larger uncertainties in the values of k_o result from the relatively minor influence of this step on the overall kinetics for all but the nickel-rich materials. Only lower limits are available for some of the chromium-rich materials since the kinetics approach first order in methane. Nevertheless, a general increase can be detected within the scatter of the data for the nickel-containing materials which is less pronounced than that for k_c. For comparison, the lines drawn through these data represent a linear dependence on surface nickel content.

SUMMARY AND CONCLUSIONS

Most of the prior kinetics studies of perovskite catalysts involved lower methane partial pressures (1–10 kPa) and somewhat higher temperatures, which were tailored to evaluate the performance of these materials as environmental remediation catalysts for deep oxidation of low-level hydrocarbon contaminants. Many of these studies include only cursory evaluation of the kinetics (rates and activation energies at one gas composition, light-off temperatures, etc.) while a few have attempted to construct rate laws and relate them to the reaction mechanism. None have reported in detail on the materials here. In the previously published studies on other $LaBO_3$ perovskites there are similarities and differences with our results. The various mechanisms which have been invoked to explain these results differ mainly in whether the reactive oxygen is supplied from the lattice and/or the gas phase, and whether the supply from the gas phase is reversible or irreversible. Several investigators have reported rate expressions which are first order in methane pressure and exhibit variable effective oxygen orders between 0 and 0.5 (13, 15, 29). This kinetic behavior has been rationalized by a model wherein oxygen is supplied by two parallel and reversible (i.e., not rate-limiting) processes: first, from the gas phase (from which oxygen orders of 0 to 0.5 arise from dissociative Langmuir adsorption) and second, from the lattice (giving a zero-order term). In some of the studies, these two oxygen sources are further associated with distinctly different TPR/TPO (3, 17, 28, 30, 33, 41), oxygen TPD (17, 35, 15, 2, 21, 23), or XPS features (1, 23, 50, 51). The MVK redox model, on the other hand, assumes that the supply of oxygen from the gas phase is irreversible, occurring only when a reduced site is made available by the reaction. This allows site oxidation to be a limiting factor in the kinetics, modifying the methane pressure dependences, consistent with the kinetic behavior seen here and in other studies. Both models are obvious oversimplifications of the actual mechanism and are not unique, but they provide useful means of evaluating kinetic data, and rationalizing the two types of kinetic behavior seen in this reaction. The oxygen and methane orders reported by Arai *et al.* (13) for $La_{0.8}Sr_{0.2}BO_x$ (B = Co, Mn) show no anticorrelation; methane orders are never less than 0.9 even though the effective oxygen orders rise to 0.5 at lower reaction temperatures. Clearly these results are not consistent with a redox mechanism like MVK. Similar findings have been reported by others (29, 15), and interestingly, all involve materials with A site substitutions. In other cases, however, consistency with MVK has been observed. In particular, the data in Figs. 6.2 and 6.3 of Ref. (15) indicate effective methane orders less than unity concurrent with finite oxygen orders for $LaFeO_3$ and $LaCoO_3$ catalysts. Analysis of the data in Figs. 6.2 and 6.3 yields $n = 0.81$, $m = 0.24$ for $LaCoO_3$ and $n = 0.75$, $m = 0.21$ for $LaFeO_3$. Additionally, the oxygen effective orders decrease with increasing temperature for $LaFeO_3$ (Fig. 6.8 in Ref. (15)), similar to our results although the corresponding methane dependences are not given. Interestingly, these materials are not substituted on the A sites. Although no deliberate variation of gas

composition was involved in their study, Klvana *et al*. (52) did report the use of the MVK rate expression to fit the conversion vs. residence time curves at various temperatures over $(La,Sr)(Ni,Co)O_3$ catalysts. The data were fit better by MVK than by the two-term model. Many other studies simply report first-order methane dependences which do not discriminate between the two models, especially at the low-methane partial pressures characteristic of these studies. Substitution on the *A* site greatly increases lattice oxygen mobility, which provides a pathway for greater reoxidation rates in these materials, and perhaps explains the distinct kinetic behavior.

The reactivity trends with nickel content can be rationalized by a simple local site model which assumes (1) that the surface oxygen species associated with two Ni cations dominate the surface activation rate, (2) that the reactivity of these species in independent of the Cr content of the material, and (3) that the distribution of Ni on the *B* sites is random. All oxygen atoms in the structure are equivalent and coordinated to two *B* cations. Ni–O–Ni ensembles in the nickel-containing materials are good candidates for the reactive species since a local defect can be formed without cation migration, i.e.,

$$Ni^{3+}–O^{2-}–Ni^{3+} \rightarrow Ni^{2+}–\square–Ni^{2+} \ (+1/2O_2). \qquad [9]$$

A random population of *B* sites by Ni ions would produce a surface density of Ni–O–Ni ensembles proportional to x^2, in agreement with the dependence found in Fig. 6. This purely statistical interpretation contains the underlying assumption that the reduction kinetics of the individuals sites are not sensitive to the overall nickel content. We also note that the onset temperature for the first wave of reduction in hydrogen (48) is similar for all the materials and the initial reduction kinetics have the same dependence on Ni content as the methane reactivities. This is undoubtedly an oversimplified interpretation—the generalized XPS shifts suggest non-local electronic changes in the materials which might influence the rate of defect formation. Furthermore, the observed rate is likely averaged over surface heterogeneity. Nevertheless, this picture is appealing. Previous studies have used both kinetic measures (TPR) and thermodynamic measures of reducibility to correlate catalytic rates. There are currently no data available regarding the thermodynamics of the reduction of $LaCr_{1-x}Ni_xO_3$ to test this alternate interpretation.

The general catalytic behavior is well explained by the foregoing simple mechanistic scheme. Not explained, however, are the remaining variations in surface reactivity both during the life of each material and between the different synthetic series. The most likely cause is variability in the detailed surface chemistry, including variable fractional coverage by the various low index planes, defects, non-statistical cation distribution, and, of course the remaining effect of small quantities of non-perovskite phases. In summary, the substitution of Cr by Ni in $LaCrO_3$ produces higher catalytic activity while preserving the inherent reduction stability of the lattice so that operation at very reducing conditions is possible, as long as the Cr/Ni ratio is greater than 1.0. Clearly, an increase in surface Ni content is a desirable goal and, if the model is correct, non-random cation distributions at the surface could also enhance the reactivity. Future investigations will examine in more detail the relationship of surface structure and reactivity and aspects of the electrocatalytic performance of the $LaCr_{1-x}Ni_xO_3$ oxides.

ACKNOWLEDGMENTS

The authors thank Chris Bertole for help in the collection of some of the rate data. Support by a Collaborative Project Grant from the Natural Sciences and Engineering Research Council of Canada (CAM) and from the Texas Center for Superconductivity and the Robert A. Welch Foundation (AJJ) is gratefully acknowledged.

REFERENCES

1. Tejuca, L. J., and Fierro, J. L. J., "Properties and Applications of Perovskite-Type Oxides," Dekker, New York, 1993.
2. Seiyama, T., *Cat. Rev.-Sci. Eng.* **34**, 281 (1992).
3. Tejuca, L. G., Fierro, J. L. G., and Tascón, J. M. D., *Adv. Catal.* **36**, 237 (1989).
4. Voorhoeve, R. J. H., *in* "Advanced Materials in Catalysis" (H. H. Burton and R. L. Garten, Eds.), p. 127. Academic Press, New York, 1977.
5. Parravano, G., *J. Am. Chem. Soc.* **75**, 1497 (1953); *J. Chem. Phys.* **20**, 342 (1952).
6. Meadowcroft, D. B., *Nature* **226**, 847 (1970).
7. Libby, W. F., *Science* **171**, 499 (1971).
8. Voorhoeve, R. J. H., Remeika, J. P., Freeland, P. E., and Matthias, B. T., *Science* **177**, 353 (1972).
9. Arakawa, J., *et al.*, *J. Catal.* **74**, 317 (1982).
10. Steele, B. C. H., Middleton, P. H., and Rudkin, R., *Solid State Ionics* **40/41**, 388 (1990).
11. Simons, T. G. E., Verhegen, E. J., Batist, P. A., and Schuit, G. C. A., *Adv. Chem. Rev.* **76**, 261 (1968).
12. Nakamura, T., Misono, M., and Yoneda, Y., *J. Catal.* **83**, 151 (1983); *Nippon Kagaku Kaishi* 1679 (1980).
13. Arai, H., Yamada, T., Eguchi, K., and Seiyama, T., *Appl. Catal.* **26**, 265 (1986).
14. McCarty, J. G., Quinlan, M. A., and Wise, H., "Proceedings, 9th International Congress on Catalysis, Calgary, 1988" (M. J. Phillips and M. Ternan, Eds.), p. 1818. Chem. Institute of Canada, Ottawa, 1988.
15. McCarty, J. G., and Wise, H., *Catalysis Today* **8**, 231 (1990).
16. Tascón, J.-M. D., Gonzales, V., and Tejuca, L. G., *React. Kinet. Catal. Lett.* **15**, 185 (1980).
17. Fierro, J. L. G., Tascón, J.-M. D., Gonzalez, L., and Tejuca, L. G., *J. Catal.* **93**, 83 (1985).
18. Choisnet, N., Abadshieva, P., Stefanov, D., Klissurski, J., Bassat, M., Rives, V., and Minchev, L., *J. Chem. Soc. Faraday Trans.* **90**, 1987 (1994).
19. Pirogova, G. N., Korovsteleva, R. I., Panich, N. M., Lagutina, T. A., and Voronin, Yu. V., *Russ. Chem. Bull.* **43**, 551 (1994).
20. Tabata, K., Matsumoto, I., Kohiki, S., and Misono, M., *J. Mater. Sci.* **22**, 4031 (1987).

21. Salomonsson, P., Griffin, T., and Kasemo, B., *Appl. Cat. A: General* **104**, 175 (1993).
22. Baiker, A., Marti, P. E., Keusch, P., Fritsch, E., and Reller, A., *J. Catal.* **146**, 268 (1994).
23. Yasuda, H., Fujiwara, Y., Mizuno, N., and Misono, M., *J. Chem. Soc. Faraday Trans.* **90**, 1183 (1994).
24. Marti, P. E., and Baiker, A., *Catal. Lett.* **26**, 71 (1994).
25. Nagamoto, H., Aanuma, K., Nobutomo, H., and Inoue, H., *Chem. Lett. (Japan)* 237 (1988).
26. Kaiji, S., Jian, L., and Yingli, B., *Catal. Lett. 1* 299 (1988).
27. Doshi, R., Alcock, C. B., Gunasekaran, N., and Carberry, J. J., *J. Catal.* **140**, 557 (1993).
28. Duprat, A. M., Alphonse, P., Sarda, C., Rousset, A., and Gillot, B., *Mat. Chem. Phys.* **37**, 76 (1994).
29. Ladavos, A., and Pomonis, P. J., *J. Chem. Soc. Farad. Trans.* 1992, 2557 (1992).
30. Baker, R. T., and Metcalfe, I. S., *Appl. Catal. A: General* **126**, 319 (1995).
31. Teraoka, Y., Zhang, H., and Yamazoe, N., *Chem. Lett. (Japan)* 1367 (1985).
32. Zhang, H. M., Shimizu, Y., Teraoka, Y., Miura, N., and Yamazoe, N., *J. Catal.* **121**, 265 (1990).
33. Du, S., Wang, J., Zheng, H., and Ma, F., *React. Kinet. Catal. Lett.* **51**, 415 (1993).
34. Kirchnerova, J., Klvana, D., Vailancourt, J., and Chaouki, J., *Catal. Lett.* **21**, 77 (1993).
35. Chan, K. S., Ma, J., Jaenicke, S., Chuah, G. K., and Lee, J. Y., *Appl. Catal. A: General* **107**, 201 (1994).
36. ten Elshof, J. E., Bouwmeester, H. J. M., and Verweij, H., *Appl. Catal. A: General* **130**, 195 (1995).
37. Steele, B. H., *Solid State Ionics* **75**, 157 (1995).
38. Appleby, A. J., and Foulkes, F. R., "Fuel Cell Handbook," Van Nostrand–Reinhold, New York, 1989.
39. Minh, N. Q., and Takahashi, T., "Science and Technology of Ceramic Fuel Cells," Elsevier, Amsterdam, 1995.
40. Middleton, P. H., Steiner, H. J., Christie, G. M., Baker, R., Metcalfe, I. S., and Steele, B. C. H., "Proceedings, 3rd International Symposium on Solid Oxide," pp. 93, 542. 1993.
41. Baker, R. T., and Metcalfe, I. S., *Appl. Catal. A: General:* **126**, 297 (1995).
42. Carter, S., Selcuk, A., Chater, R. J., Kajda, J., Kilner, J. A., and Steele, B. C. H., *Solid State Ionics* **53–56**, 597 (1992).
43. Anderson, H. U., *Solid State Ionics* **52**, 33 (1992).
44. Ishihara, T., Matsuda, H., and Takita, Y., *J. Am. Chem. Soc.* **116**, 3801 (1994).
45. Ishihara, T., Matsuda, H., and Takita, Y., *Solid State Ionics* **79**, 147 (1995).
46. Ganguly, P., Vasanthacharya, N. Y., Rao, C. N. R., and Edwards, P. P., *J. Solid State Chem.* **54**, 400 (1984).
47. Höfer, H. E., and Schmidberger, R., *J. Electrochem. Soc.* **141**, 782 (1994).
48. Stojanovic, M., Haverkamp, R. G., Mims, C. A., Moudallal, M., and Jacobson, A. J., *J. Catal.* **166**, 315 (1997).
49. Mars, P., and van Krevelen, D. W., *Special Supplement, Chem. Eng. Sci.* **3**, 41 (1954).
50. Tejuca, L. G., and Fierro, J. L. G., *Thermochimica Acta* **147**, 361 (1989).
51. Fierro, J. L. G., and Tejuca, L. G., *Appl. Surf. Sci.* **27**, 453 (1987).
52. Klvana, D., Vaillancourt, J., Kirchnerova, J., and Chaouki, J., *Appl. Catal. A: General* **109**, 181 (1994).